Pergamon

PII: S0277-5387(97)00041-7

Polyhedron Vol. 16, No. 17, pp. 3013–3031, 1997

0277-5387/97 $17.00+0.00

Synthesis, identification and thermal analysis of coprecipitates of silver-(cobalt, nickel, copper and zinc) oxalate

Ahmed M. Donia

Department of Chemistry, Faculty of Science, Menoufia University, Shebin El-Kom, Egypt

(Received 7 May 1996; accepted 16 January 1997)

Abstract—The coprecipitates $Ag_2M(C_2O_4)_2 \cdot nH_2O$ ($M = Co^{2+}$, Ni^{2+}, Cu^{2+} or Zn^{2+}) have been prepared and identified by means of IR, elemental analysis, XRD, SEM and (DTA/TGA). The XRD and SEM data indicate that, the coprecipitates are solid solutions. The thermal decomposition of the compounds in dynamic air and N_2 flow has been studied. It is established that, the atmosphere plays a significant role upon the nature of decomposition as well as the type of thermoproducts and their thermal stability. The present study gives also an idea about the nature of interaction of the water of crystallization. The mixed oxide obtained from the thermal decomposition of $Ag_2Ni(C_2O_4)_2 \cdot 2H_2O$ in air and N_2 has been investigated. The XRD and SEM results suggest the formation of a mixed lattice oxide Ag_2NiO_2. © 1997 Elsevier Science Ltd

Keywords: synthesis; thermal analysis; oxalates; coprecipitates.

In recent years, the quest for high purity ceramic materials for the electronics industry had led to the wide use of sol-gel [1] and coprecipitation techniques [2,3]. In the precipitation–filtration technique, the metal ions are simultaneously precipitated in the expected stoichiometric proportions. Thereafter the precipitate is filtered off, washed and dried. In a number of cases a single phase solid solution precipitates assuring homogeneity. However, even if segregation occurs during precipitation the degree of mixing is far superior to that obtained with conventional mixing techniques. One of the most used precipitating agents is the oxalate ion. Oxalates form solid solutions and can easily be decomposed [4]. The preparation and thermal investigation of silver [5–8], cobalt and nickel [9,10], copper [9,11] and zinc [12] oxalates were previously reported. On the other hand, the bimetal oxalate solid solutions have also been prepared and studied by Wickham [13] and Robin [14]. Schuele [15] successfully prepared Co—Fe, Ni—Fe, Zn—Fe, Mg—Fe and Mn—Fe oxalate solid solutions, but failed with the Cu—Fe system. He concluded that ions with nearly the same ionic radii can form solid solutions with each other. Recently, the solid solutions of Ni—Co oxalate have been prepared and studied [10,16]. The results obtained indicated that, due to the similarity of both the charge and solid state ionic radii of nickel and cobalt ions, there is a complete range of solid solution and very little change in the lattice with composition. We also prepared and identified the solid solution of Co—Cu oxalate [17] (in which cobalt and copper have somewhat different ionic radii). The results reveal only the formation of solid solution with composition of high cobalt content (high ionic radius). In the present study, the coprecipitates of silver-(cobalt, nickel, copper or zinc) oxalate (in which both the charge and ionic radii are different) have been prepared and identified, the study has also thrown light on the thermal decomposition of the compounds in both air and N_2 atmospheres.

EXPERIMENTAL

Materials

$AgNO_3$, $Co(NO_3)_2 \cdot 6H_2O$, $Ni(NO_3)_2 \cdot 6H_2O$, $Cu(NO_3)_2 \cdot 2.5H_2O$ and $Zn(NO_3)_2 \cdot 6H_2O$ were obtained from Fisher Scientific. Oxalic acid was obtained from J. T. Baker Chemical Co. All the compounds were chemically pure, and were used without further purification.

Method

Distilled water (250 cm^3) and 0.1 M oxalic acid solution (25 cm^3) were mixed together in a large beaker. A 0.1 M solution (300 cm^3) mixture of silver nitrate and cobalt, nickel, copper or zinc nitrate in the required molar ratio (2:1) of Ag^+ and M^{2+}, respectively was added simultaneously and dropwise with a 0.1 M oxalic acid solution (175 cm^3) to the solution already present in the beaker with stirring and warming (about 50°C). The addition was completed in 1 h, and followed by another 4 h stirring. The reacted solution was then left until all the precipitate had settled. The remaining clear solution was decanted off. The precipitate was then filtered and washed several times with distilled water sequentially with ethyl alcohol. The precipitate was carefully dried in air during the filtration, and was then left to dry over anhydrous $CaCl_2$ for one week before investigation. The single oxalates were prepared by the same method. The C and H analyses (Table 1) were in good agreement with the formulae

$Ag_2M(OX)_2 \cdot nH_2O$;		($OX = C_2O_4^{-2}$)
$M = Co^{2+}$;	$n = 2$	(1)
$M = Ni^{2+}$;	$n = 2$	(2)
$M = Cu^{2+}$;	$n = 0.3$	(3)
$M = Zn^{2+}$;	$n = 2$	(4)

The formulae of the single oxalates are $Ag_2(OX)$, $Co(OX) \cdot 2H_2O$, $Ni(OX) \cdot 2.5H_2O$, $Cu(OX) \cdot 0.3H_2O$ and $Zn(OX) \cdot 2H_2O$.

The number of molecules of water of crystallization were also confirmed by TG weight loss. The infrared (IR) spectra of the compounds showed similar patterns in the wavenumber range 4000–500 cm^{-1}, indicating that oxalate group were coordinated to all the metal ions under study in a similar fashion. The spectra displayed bands at 3370 (s/br) (except 3), 1650 (vs), 1350 (m), 1315 (s), 850 (m), 770 (s), 630 (m) and 530 (m) cm^{-1}. These bands are assigned [18,19] to ν(OH), ν_{as}(C=O), ν_{sym}(C—O)+ν(C—C), ν_{sym}(C—O)+δ(O—C=O), ν(O—M—O), δ(O—C=O)+ν(M—O), ν(O—M—O) and ν(M—O)+ν(C—C). The bidentate linkage of the oxalate group with the metal was confirmed on the basis of the difference between the antisymmetric and symmetric stretching frequencies [19].

Table 1. Elemental analysis of single oxalates and their coprecipitates

Compound	C(%)	H(%)
$Co(OX) \cdot 2H_2O$	13.1(13.1)	2.2(2.1)
$Ni(OX) \cdot 2.5H_2O$	12.5(12.5)	2.6(2.6)
$Cu(OX) \cdot 0.3H_2O$	15.2(15.1)	0.4(0.4)
$Zn(OX) \cdot 2H_2O$	12.7(12.7)	2.1(2.1)
$Ag_2(OX)$	7.9(7.9)	—
$Ag_2Co(OX)_2 \cdot 2H_2O$	9.8(9.7)	0.8(0.7)
$Ag_2Ni(OX)_2 \cdot 2H_2O$	9.8(9.7)	0.8(0.8)
$Ag_2Cu(OX)_2 \cdot 0.3H_2O$	10.4(10.3)	0.1(0.1)
$Ag_2Zn(OX)_2 \cdot 2H_2O$	9.7(9.7)	0.8(0.8)

Found analyses in parentheses.

Measurements

The X-ray powder diffraction (XRD) was carried out on a Scintag XDS 2000 powder diffraction with K_α radiation, $\lambda = 1.540598$, using a solid state Ge detector cooled by liquid nitrogen. The experimental conditions for all patterns taken were: working voltage, 45 kV; working current, 40 mA; $2\theta = 5$–$70°$; scan with speed of 3.0° min^{-1} and a 0.03° step for intensity integration. The measurements were taken at room temperature in air. The data were processed using Scintag software DMS version 2.0 on Micro VAX 3100 with a Tektronix terminal. The elemental analysis (C,H) were performed using a Perkin Elmer 2400 elemental analyzer (University of Toledo, U.S.A). IR spectra were recorded on a Nicolet 5DX FTIR spectrophotometer using KBr discs technique. The scanning electron microscopic studies were carried out on a JEOL JSM 6100 scanning electron microscope. The surface of the sample was coated with a thin uniform, electrically conductive gold film. The thermal analysis (DTA/TG) was measured on a SDT 2960 simultaneous TGA-DTA TA Instrument 2000. The experiments were carried out at a heating rate of 10°C min^{-1} in both dynamic air and N_2 (flow of 50 cm^3 min^{-1}).

RESULTS AND DISCUSSION

The X-ray patterns of the single oxalates; and the coprecipitates and their mechanical mixtures (with the same mole ratio) are shown in Fig. 1(a) and (b). The X-ray data (2θ *vs* d spacing and intensity) are collected in Table 2. Both single oxalates and coprecipitates are characterized by higher degree of crystallinity. The intensive investigation of the patterns gave the following points:

(1) Generally the feature of the patterns of the mechanical mixtures is very different from that of the coprecipitates.

(2) The two lines of silver oxalate $2\theta = 29.7928°$ (most intense line d = 2.99643 Å) and $2\theta = 32.3241°$ (d = 2.7673 Å) are predominant (and appear exactly at the same position) in all patterns of the mechanical mixtures.

(3) The lines of silver oxalate are also predominant in the patterns of coprecipitates whereas the lines of cobalt, nickel copper and zinc oxalates suffer from lower intensities. As indicated from d-spacing values (Table 2), the lines of coprecipitates are generally shifted in positions from those of their single oxalates. This shift may be attributed to the distribution of the

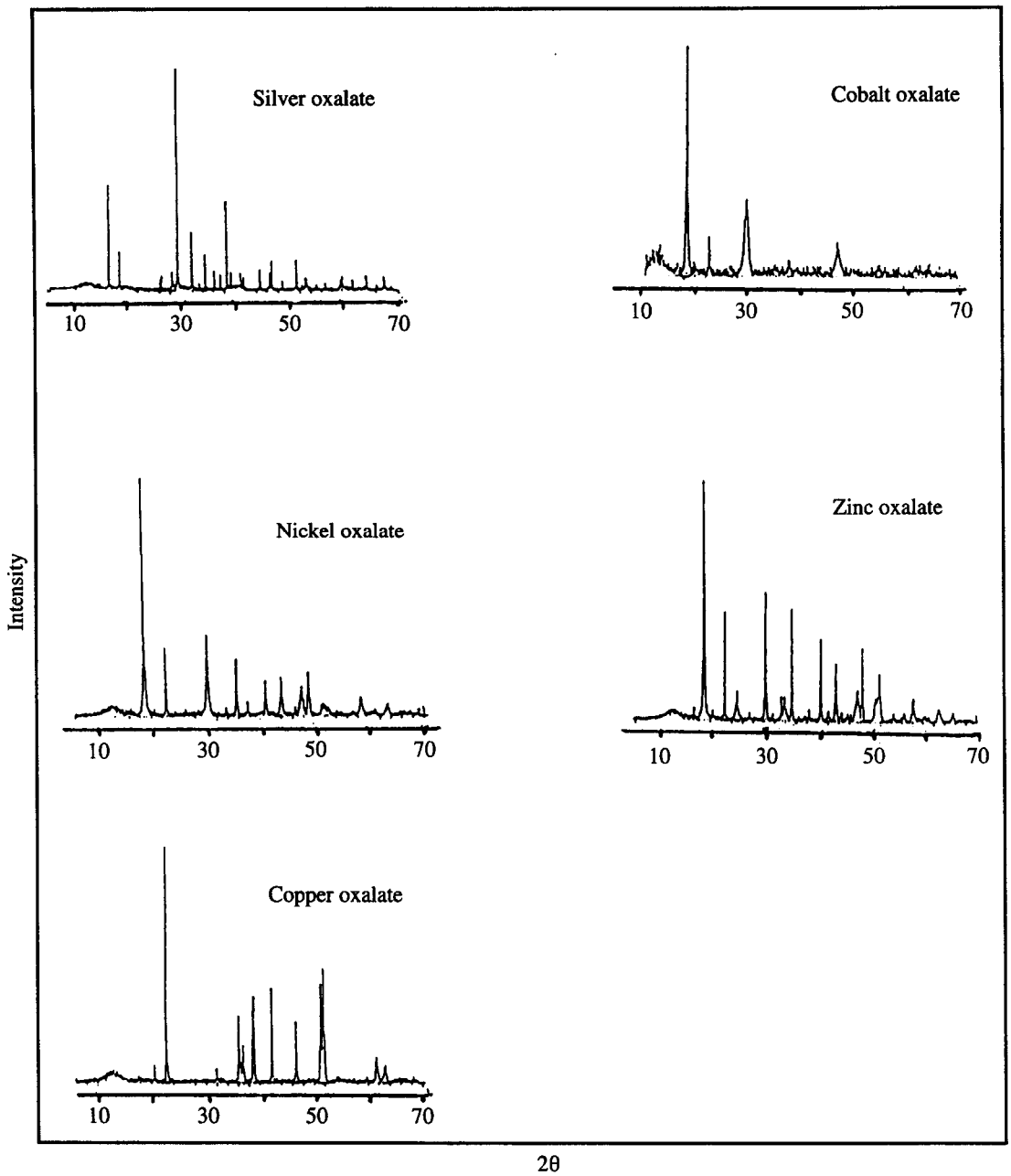

Fig. 1. (a) X-ray diffraction patterns of single oxalates.

metal ions (Co^{2+}, Ni^{2+}, Cu^{2+} or Zn^{2+}) in the lattice of silver oxalate forming the solid solutions [15,20]. On the other hand, the most intense line of silver oxalate shifts on coprecipitation from d = 2.99643 Å to d = 2.31651, 2.76369 and 2.32001 Å for cobalt, nickel and zinc coprecipitates, respectively. This indicates the appearance of a new phase as a result of the formation of the solid solution.

The formation of the solid solutions can also be confirmed from the results of SEM. The micrographs of the single oxalates are displayed in Fig. 2(a). As reported earlier, cobalt oxalate [10,17] contained rod-like particles of the order of about 20 μm in length and about 2 μm in width. Copper oxalate [17] particles are similar and have a uniform thin circular plate-like with radius of about 2.8 μm. Nickel oxalate [10] has rounded particles with radius of about 2.5 μm. Silver oxalate shows different particle morphology. The material contains larger particles, with a mixture of particle shapes and sizes. The investigation of the micrograph of zinc oxalate indicates that it contains similar uniform cubic particles of size 148 μm^3 (see the fragmented particles). These cubic particles associated together through their edges to give the observed uniform cluster-like shape particles. Fig. 2(a) shows also the micrograph of the mechanical mixture of silver

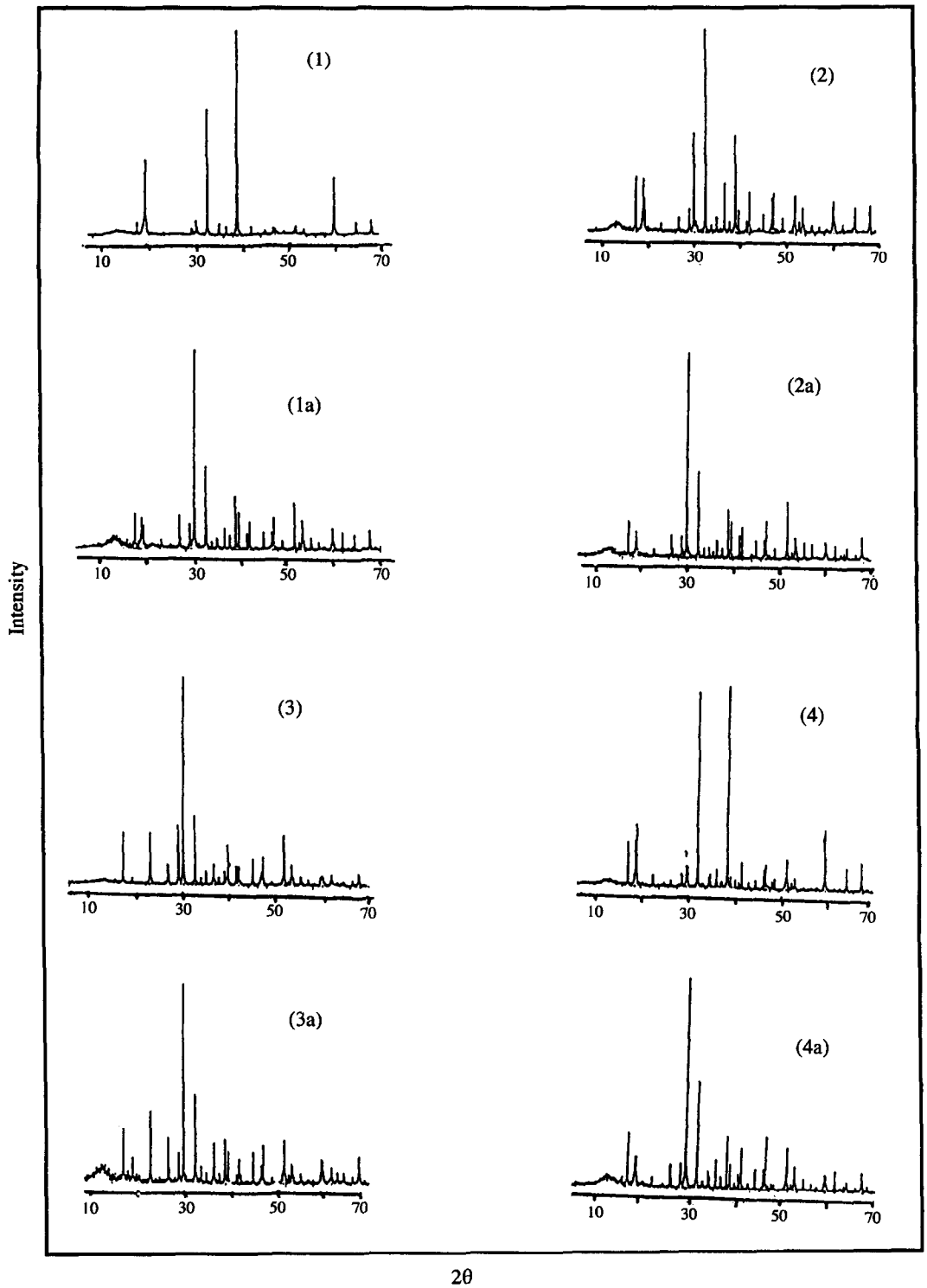

Fig. 1. (b) X-ray diffraction patterns of coprecipitates (1), (2), (3) and (4); and their mechanical mixtures (1a), (2a), (3a) and (4a).

oxalate and nickel oxalate with the same mole ratio of their coprecipitate, (2a); which was selected as an example of the mechanical mixtures. It can be seen that, the micrograph appears as a mixture of particles of silver oxalate and nickel oxalate. This is in conformity with our previous work [17]. In contrast, the micrographs of the coprecipitates (Fig. 2(b)) show no particles corresponding to their single oxalates, thereby indicating the formation of the solid solutions. The micrograph of the coprecipitate of cobalt (1) for

Table 2. X-ray diffraction data of the coprecipitates

$Ag_2Co(OX)_2 \cdot 2H_2O$			$Ag_2Ni(OX)_2 \cdot 2H_2O$			$Ag_2Cu(OX)_2 \cdot 0.3H_2O$			$Ag_2Zn(OX)_2 \cdot 2H_2O$		
	d-spacing			d-spacing			d-spacing			d-spacing	
2θ	(Å)	(I/I^c)	2θ	(Å)	(I/I^c)	2θ	(Å)	(I/I^c)	2θ	(Å)	(I/I^c)
12.1878	7.25614	2	12.8175	6.90105	5	17.2269	5.14331	23	11.6825	7.56884	2
12.7487	6.93811	3	13.0037	6.80262	5	19.1628	4.62785	3	12.3200	7.17858	2
12.9791	6.81551	2	17.2547	5.13509	28	22.9284	3.87561	24	12.4850	7.08408	2
13.4272	6.58903	2	18.8984	4.69199	28	26.5666	3.35254	9	12.9697	6.82041	2
14.0622	6.29289	3	19.1628	4.62785	17	26.9106	3.31046	5	13.1287	6.73813	3
14.6325	6.04888	2	26.5900	3.34964	7	28.8103	3.09635	27	13.3991	6.60280	3
14.8397	5.96489	2	28.8266	3.09464	11	29.8444	2.99137	100	13.5962	6.50748	3
17.2666	5.13158	6	29.8491	2.99092	49	32.3563	2.76465	31	13.8481	6.38968	2
18.4384	4.80799	5	30.4169	2.93636	6	34.7984	2.57601	6	14.0191	6.31215	2
18.8472	4.70463	31	32.3678	2.76369	100	36.4762	2.46128	10	14.6481	6.04246	2
19.1844	4.62270	37	34.8366	2.57328	8	37.5994	2.39030	4	17.2075	5.14906	21
28.8253	3.09477	3	36.4978	2.45988	25	38.8122	2.31835	6	18.7806	4.72116	23
29.1772	3.05824	2	37.6200	2.38904	5	39.2675	2.29252	3	19.1275	4.63631	30
29.8641	2.98945	7	38.8213	2.31783	47	39.5537	2.27658	18	22.6500	3.92262	6
30.2309	2.95400	4	39.5634	2.27605	10	41.3159	2.18346	8	26.5225	3.35801	3
32.3756	2.76304	62	41.3081	2.18386	5	41.9078	2.15398	9	28.7834	3.09918	6
34.9509	2.56512	5	41.8922	2.15475	19	44.9131	2.01658	12	29.1253	3.06357	5
36.4956	2.46002	4	44.9234	2.01614	8	46.6434	1.94572	6	29.8056	2.99518	17
38.8444	2.31651	100	46.6522	1.94538	15	47.1225	1.92705	13	30.2422	2.95293	10
41.9016	2.15429	4	47.1331	1.92664	19	51.6444	1.76845	22	32.3234	2.76738	93
46.6516	1.94540	3	49.0409	1.85606	6	53.2863	1.71776	9	34.8894	2.56951	6
47.1475	1.92609	3	51.6331	1.76881	18	55.3294	1.65907	4	35.1300	2.55246	6
51.6291	1.76894	4	52.6128	1.73815	5	59.7222	1.54710	4	36.4381	2.46377	9
53.3194	1.71677	2	53.2944	1.71752	11	60.0716	1.53894	4	37.5622	2.39258	3
59.7884	1.54554	27	59.7606	1.54620	15	61.9278	1.49719	5	38.7834	2.32001	100
64.4812	1.44393	6	64.4756	1.44404	12	67.6603	1.38361	6	39.5069	2.27917	5
67.6719	1.38340	7	67.6506	1.38378	14				40.5403	2.22343	4
									41.2741	2.18558	2
									41.8547	2.15659	12
									43.4516	2.08096	3
									44.8859	2.01774	4
									46.6034	1.94730	9
									47.0828	1.92859	11
									48.4241	1.87826	3
									49.0078	1.85724	5
									51.3669	1.77735	5
									51.5981	1.76992	13
									52.5897	1.73886	3
									53.2644	1.71842	5
									59.7322	1.54687	29
									64.4272	1.44501	10
									64.5972	1.44161	5
									67.6181	1.38437	13
									67.7988	1.38112	7

example, contained similar large thin sheet particles (with some fragments) of the order of about 53 μm in length and 33 μm in width. The micrograph of the coprecipitate of nickel (2) shows also the thin sheet particles (16 μm in length and 7.8 μm in width) along with fragmented particles. The photos of the coprecipitates of copper (3) and zinc (4) are characterized by different particle shapes and sizes. These results confirm the formation of the solid solutions and are compatible with their polycrystalline nature obtained from XRD patterns.

Thermal investigation

The DTA and TG curves of the solid solutions (1), (2), (3) and (4) in both air and N_2 are given in Figs. 3(a), (b), (c) and (d), respectively. The thermal analysis data together with the products of the thermal reactions are recorded in Table 3. As seen in Figs. 3(a) and (d) and Table 3, the solid solutions of cobalt (1) and zinc (4) show loss of the water of crystallization in two steps. The first molecule was lost in an individual step whereas the second loss occurred during

nickel oxalate

silver oxalate

Fig. 2. (a) SEM of single oxalates and mechanical mixture, (2a), of silver oxalate and nickel oxalate.

cobalt oxalate

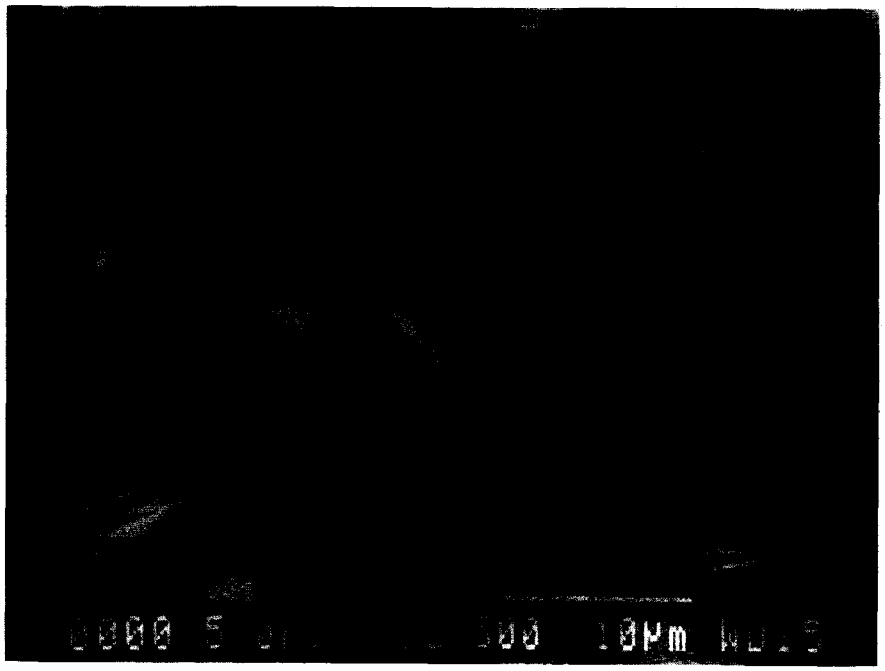

copper oxalate

Fig. 2(a)—*continued.*

zinc oxalate

mechanical mixture of silver oxalate and nickel oxalate (2a)

Fig. 2(a)—*continued.*

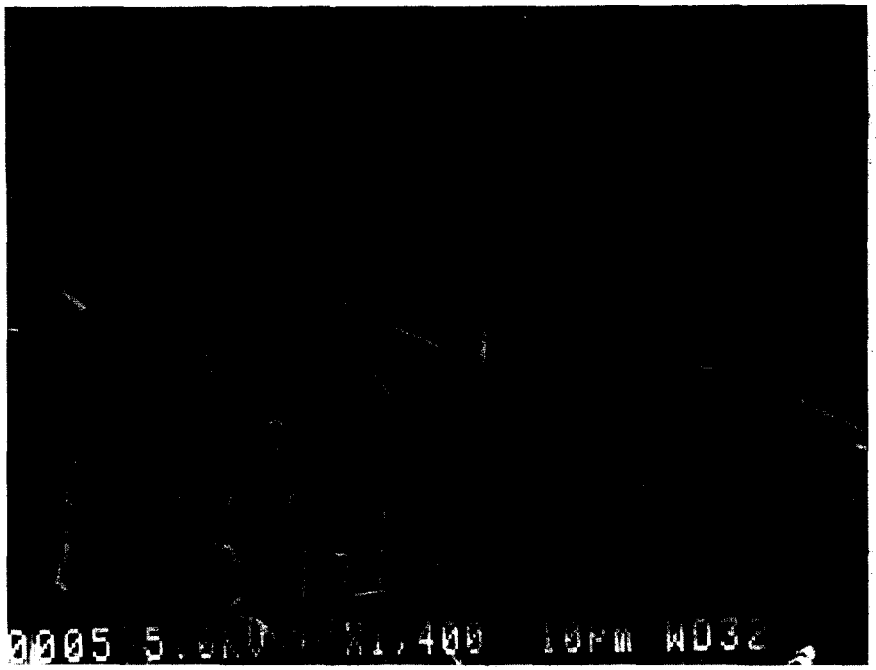

(1)

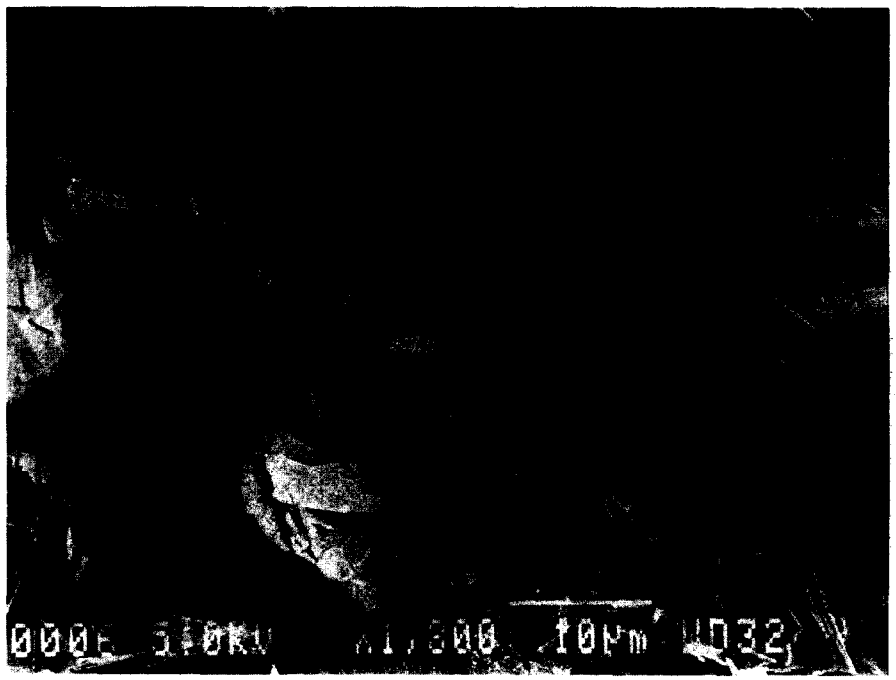

(2)

Fig. 2. (b) SEM of coprecipitates (1), (2), (3) and (4).

(3)

(4)

Fig. 2(b)—*continued.*

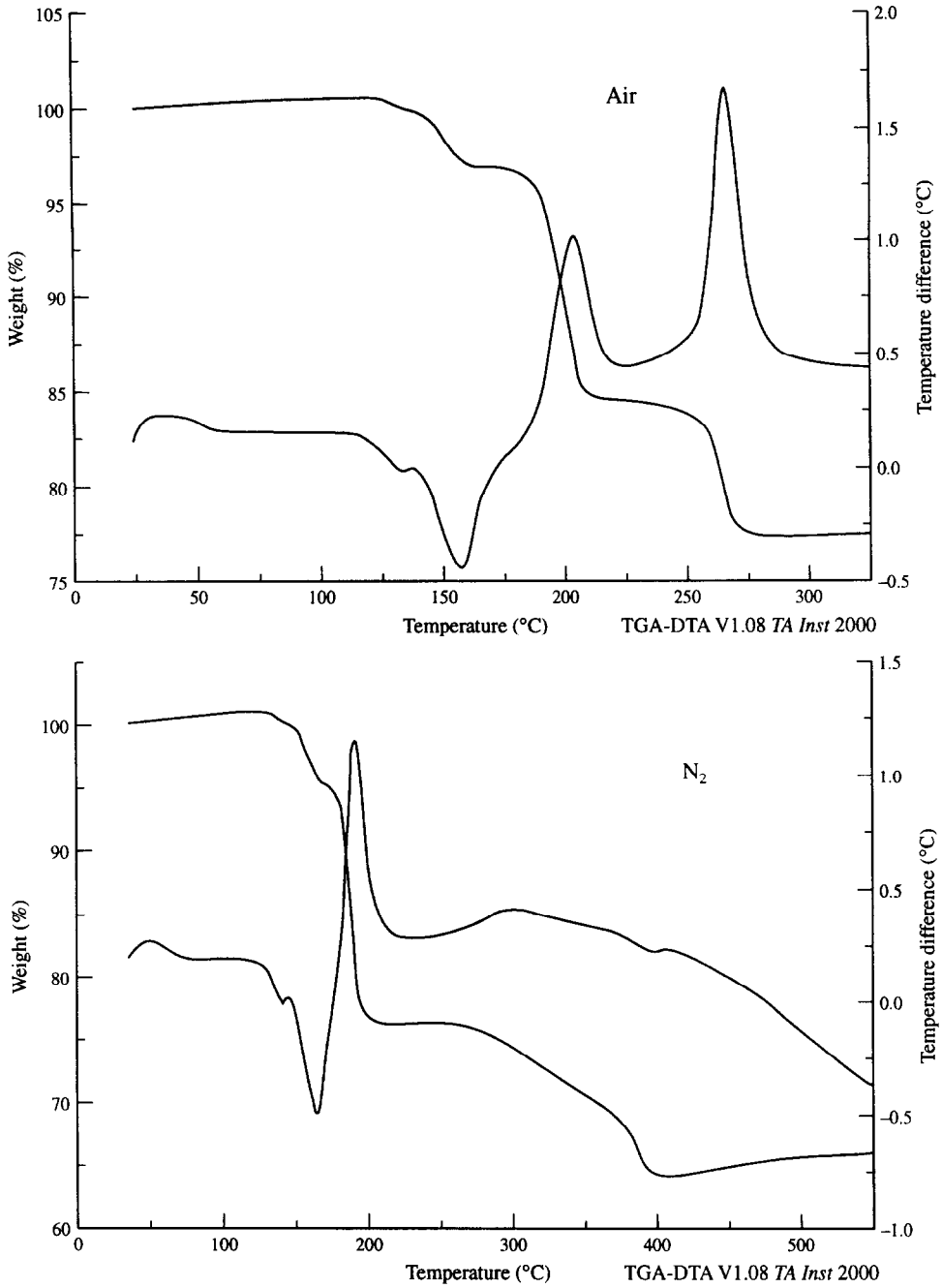

Fig. 3. (a) DTA and TG curves of solid solution (1) in air and N_2.

the decomposition. This indicates the different nature of the interaction of the water of crystallization in the lattices of those solid solutions. For the solid solutions of nickel (2) and copper (3), the water was lost during the decomposition and at a relatively high temperature to that of (1) and (4), indicating the higher interaction of the water in the lattices of (2) and (3). In addition to the DTA and TG data, the decomposition processes of the compounds were confirmed from the IR spectra of the heated compounds up to the corresponding temperatures. The spectra are characterized by the disappearance of characteristic peaks of the oxalate group.

$Ag_2Co(OX)_2 \cdot 2H_2O$

The observed two overlapping endothermic DTA peaks in the temperature range 115–185°C in both air and N_2 atmosphere (Fig. 3(a)) are assigned to loss of one molecule of water of crystallization. This assignment was confirmed by the TG weight losses in that

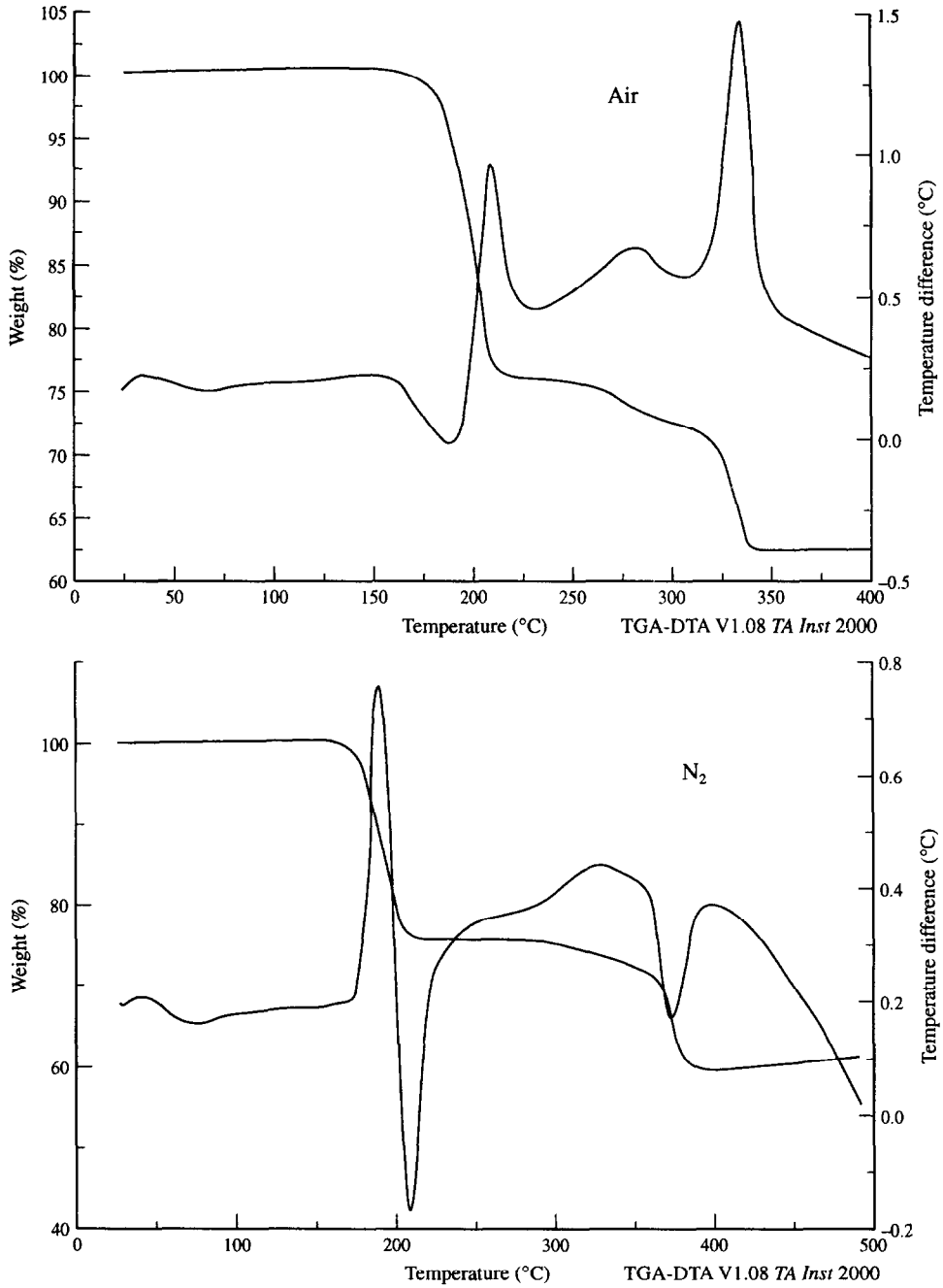

Fig. 3. (b) DTA and TG curves of solid solution (2) in air and N_2.

temperature range (Table 3). As indicated from the thermal data, the second water molecule was lost during the decomposition of the compound. This behaviour together with the observed overlapping nature of the endothermic dehydration DTA peak, indicating the different nature of interaction of the water of crystallization in the lattice. In air, the trace also shows exothermic peaks in the range 185–270°C. As shown from the corresponding TG weight losses in that temperature range, the first peak (max. 205°C) is assigned to the loss of the second molecule of water together with the decomposition of the compound to give the oxycarbonate $[Ag_2CoO(CO_3)_2]$ at 215°C. The second peak (mix. 268°C) is assigned to the completion of decomposition reaction to give finally the stable trioxycarbonate $[Ag_2CoO_3(CO_3)]$ at 270°C, in which the oxidation state of the metal ions is being raised. The compound in N_2 atmosphere shows different decomposition behaviour in the temperature range 163–400°C. As shown from the TG data (Table 3), the first exothermic DTA peak (mix. 187°C) is assigned to the loss of the second molecule of water together with

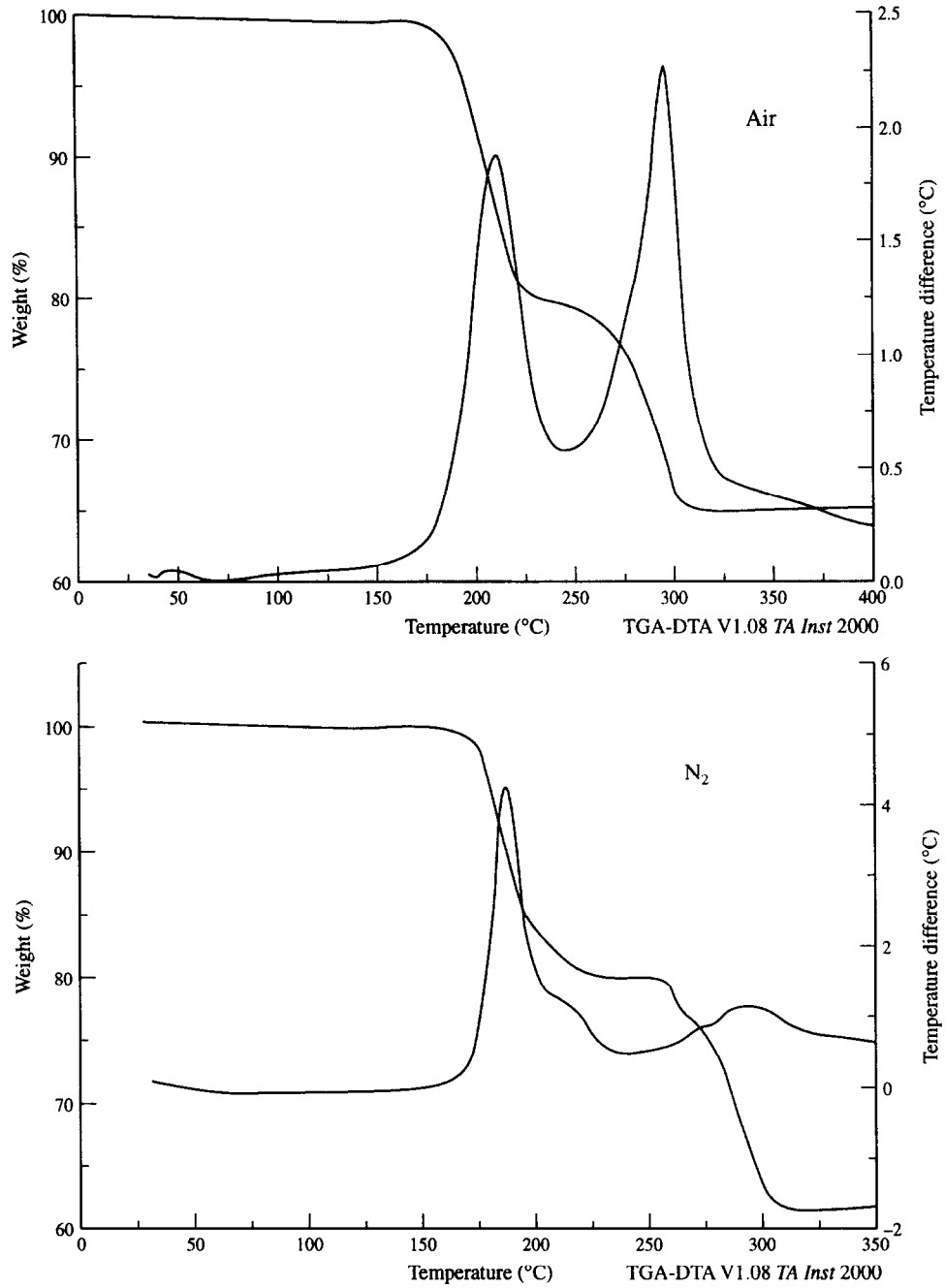

Fig. 3. (c) DTA and TG curves of solid solution (3) in air and N_2.

the decomposition of the compound to give the oxygen rich dioxycarbonate phase $Ag_2CoO_{2.25}(CO_3)$ at 205°C. This phase is stable up to 250°C (Fig. 3(a)). Then it starts to decompose through successive weak exothermic (300°C) and endothermic (395°C) events to give finally the stable oxide ($Ag_2CoO_{2.5}$) at 400°C. The TG data (Table 3 and Fig. 3(a)) indicate that, the formation of the stable oxide takes place through the formation of unstable intermediate $Ag_2CoO_2(CO_3)$ at 285°C. It is clear that the oxygen rich phase $Ag_2CoO_{2.25}(CO_3)$ displays thermal stability on comparison with the dioxycarbonate phase $[Ag_2CoO_2(CO_3)]$.

$Ag_2Ni(OX)_2 \cdot 2H_2O$

This compound displays different thermal behaviour in air and N_2 atmospheres. All thermal events are inversed on transfer from air to N_2 (Fig. 3(b)). In air, the TG weight losses in the range 150–215°C indicate that the two successive endothermic (178°C) and exo-

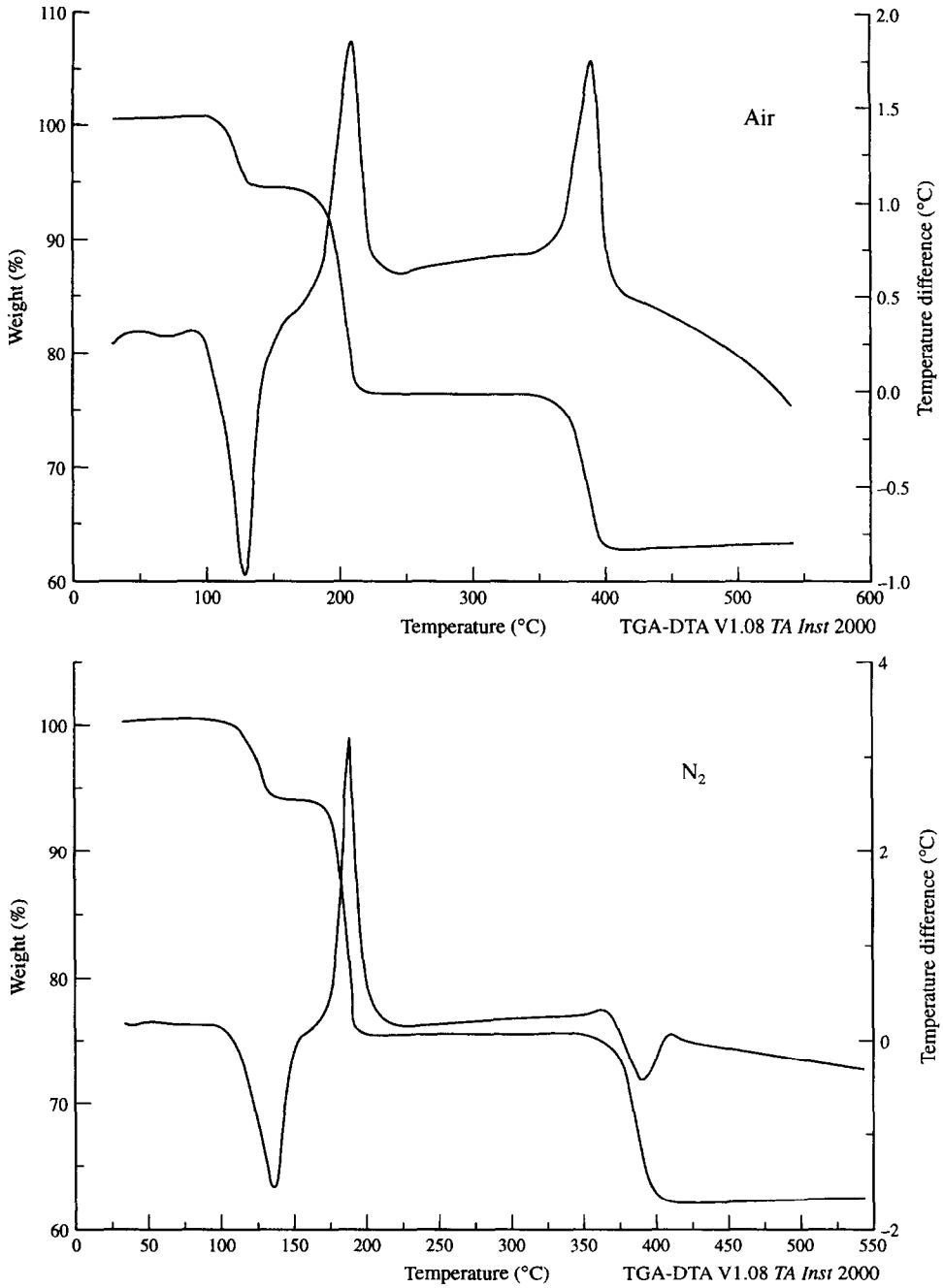

Fig. 3. (d) DTA and TG curves of solid solution (4) in air and N_2.

thermic (210°C) events are characteristic by loss of water of crystallization together with the decomposition of the compound to give the oxygen rich dioxycarbonate [$Ag_2NiO_{2.25}(CO_3)$] at 215°C. This compound shows thermal stability up to 250°C and then starts to decompose through successive exothermic events with maxima at 285°C and 335°C, respectively. The TG data indicate the formation of a stable oxide Ag_2NiO_2 at 340°C through the formation of unstable oxycarbonate $Ag_2NiO(CO_3)$ intermediate at 315°C. In the N_2 atmosphere, the observed successive exothermic (185°C) and endothermic (210°C) peaks in the range 160–235°C are assigned to the decomposition together with loss of water of crystallization. On the basis of TG weight losses (Table 3), the decomposition reaction gives the oxygen rich dioxycarbonate phase [$Ag_2NiO_{2.25}(CO_3)$] at 210°C. This phase is also thermally stable up to 250°C, and then starts to decompose endothermally in the region 250–400°C. As indicated from the TG data, the broad endothermic peak in the range 260–310°C corresponds to the formation of unstable dioxycarbonate

Table 3. TG data of the solid solutions

Compound	Temp. range (°C)	Weight loss % Cal. (F)	Reaction	Products
$Ag_2Co(OX)_2 \cdot 2H_2O$				
Air:	115–185	3.7(3.5)	a	H_2O
	185–215	11.9(11.8)	a+b	$Ag_2CoO(CO_3)_2$
	240–270	5.7(5.7)	b	$Ag_2CoO_3(CO_3)$
N_2:	115–163	3.7(3.8)	a	H_2O
	163–205	20.1(20.0)	a+b	$Ag_2CoO_{2.25}(CO_3)$
	250–285	0.8(0.8)	b	$Ag_2CoO_2(CO_3)$
	285–400	10.6(10.6)	b	$Ag_2CoO_{2.5}$
$Ag_2Ni(OX)_2 \cdot 2H_2O$				
Air:	150–215	23.9(23.8)	b	$Ag_2NiO_{2.25}(CO_3)$
	250–315	4.1(4.3)	b	$Ag_2NiO(CO_3)$
	315–340	9.0(9.2)	b	Ag_2NiO_2
N_2:	160–210	23.9(23.9)	b	$Ag_2NiO_{2.25}(CO_3)$
	250–295	0.8(0.8)	b	$Ag_2NiO_2(CO_3)$
	295–378	12.3(12.1)	b	Ag_2NiO_2
$Ag_2Cu(OX)_2 \cdot 0.3H_2O$				
Air:	180–225	19.5(19.5)	b	$Ag_2CuO_2(CO_3)$
	225–305	14.7(14.9)	b	$Ag_2CuO_{1.5}$
N_2:	170–220	19.5(19.7)	b	$Ag_2CuO_2(CO_3)$
	255–265	3.5(3.4)	b	$Ag_2CuO(CO_3)$
	265–292	9.5(9.3)	b	Ag_2CuO_2
	292–300	3.5(3.4)	b	Ag_2CuO
	300–315	1.7(1.8)	b	$Ag_2CuO_{0.5}$
$Ag_2Zn(OX)_2 \cdot 2H_2O$				
Air:	100–125	3.7(3.7)	a	H_2O
	175–205	15.0(14.5)	a+b	$Ag_2Zn(CO_3)_2$
	365–400	17.8(17.9)	b	Ag_2ZnO_2
N_2:	100–128	3.7(3.8)	a	H_2O
	170–185	15.0(15.5)	a+b	$Ag_2Zn(CO_3)_2$
	365–398	17.8(17.7)	b	Ag_2ZnO_2

a = dehydration, b = decomposition

$Ag_2NiO_2(CO_3)$ at 295°C. This dioxycarbonate is spontaneously decomposed endothermally (Fig. 3(b)) to give finally the oxide Ag_2NiO_2 at 378°C. It is noteworthy that, the oxygen rich dioxycarbonate phases of both cobalt and nickel are formed in the same range and display the same range of stability. They also decomposed through the formation of unstable intermediates to give $Ag_2CoO_{2.5}$ (for cobalt) and Ag_2NiO_2 (for nickel).

$Ag_2Cu(OX)_2 \cdot 0.3H_2O$

Fig. 3(c) shows a different decomposition nature of the compound in both air and N_2 atmosphere. In air, the compound starts to decompose at 180°C. The decomposition proceeds through successive exothermic events at 210°C and 295°C, respectively. The TG weight losses (Table 3) infer the formation of the dioxycarbonate $Ag_2CuO_2(CO_3)$ at 225°C. This dioxycarbonate gradually decomposes exothermally in the region 225–305°C to give the stable (oxygen deficient) oxide $Ag_2CuO_{1.5}$ at 305°C. In N_2 atmosphere, the compound decomposed in the range 170–220°C through successive exothermic events at 188°C and 215°C, respectively. The TG data indicates the formation of dioxycarbonate at 220°C. This compound shows thermal stability up to 255°C, and then starts to decompose exothermally in two steps in the range 255–310°C. The TG data shows that, the first step corresponds to the formation of unstable oxycarbonate $Ag_2CuO(CO_3)$ at 265°C, which in turn decomposed through the formation of unstable intermediates Ag_2CuO_2 (292°C) and Ag_2CuO (300°C) to give finally the stable (highly oxygen deficient) $AgCuO_{0.5}$ form at 315°C. It is seen that, the dioxycarbonate [$Ag_2CuO_2(CO_3)$], which formed during the thermal decomposition of the compound shows different thermal characteristics in both air and N_2 atmospheres. Also, the finally obtained oxides are nonstoichiometric and characterized by oxygen deficient.

$Ag_2Zn(OX)_2 \cdot 2H_2O$

As shown in Fig. 3(d), the thermal behaviour of this compound is characterised by three events in both air and N_2 atmospheres. As indicated from the TG

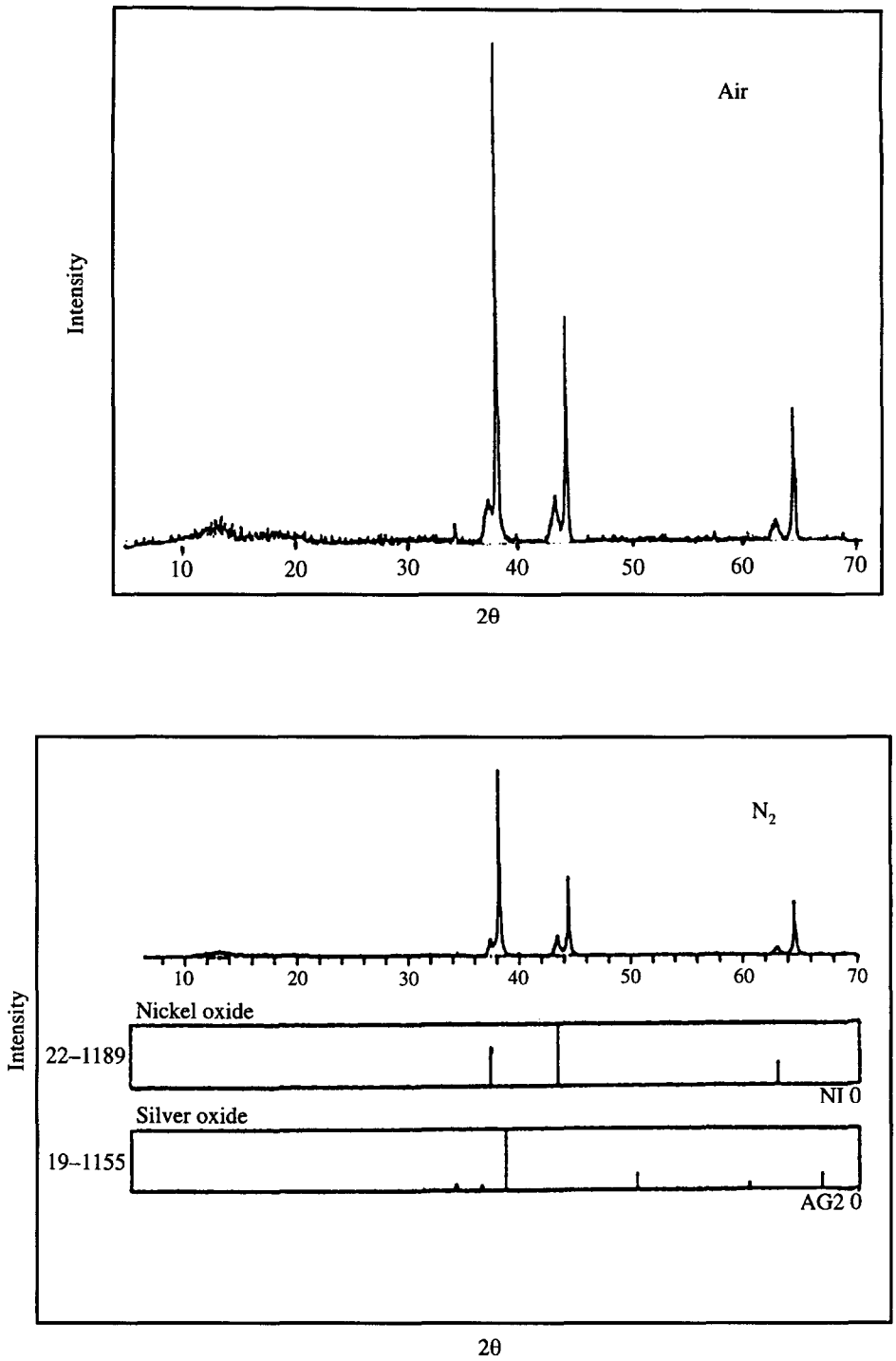

Fig. 4. X-ray diffraction patterns of Ag_2NiO_2 obtained from the thermal decomposition of coprecipitate (2) in air and N_2 up to 500°C; and Ag_2O and NiO.

data in the region 100–205°C (Table 3), the first endothermic peak at 130°C is assigned to the loss of one molecule of water of crystallization. The second endothermic peak at 205°C (air) and 185°C (N_2) is assigned to loss of the second water molecule together with the decomposition to give the carbonate $Ag_2Zn(CO_3)_2$. This carbonate shows thermal stability up to 365°C in both air and N_2, and then starts to decompose in the range 365–400°C (third event at 390°C) to give finally the stable oxide Ag_2ZnO_2. It is seen, the decomposition reaction of carbonate is exothermic in air and endothermic in N_2.

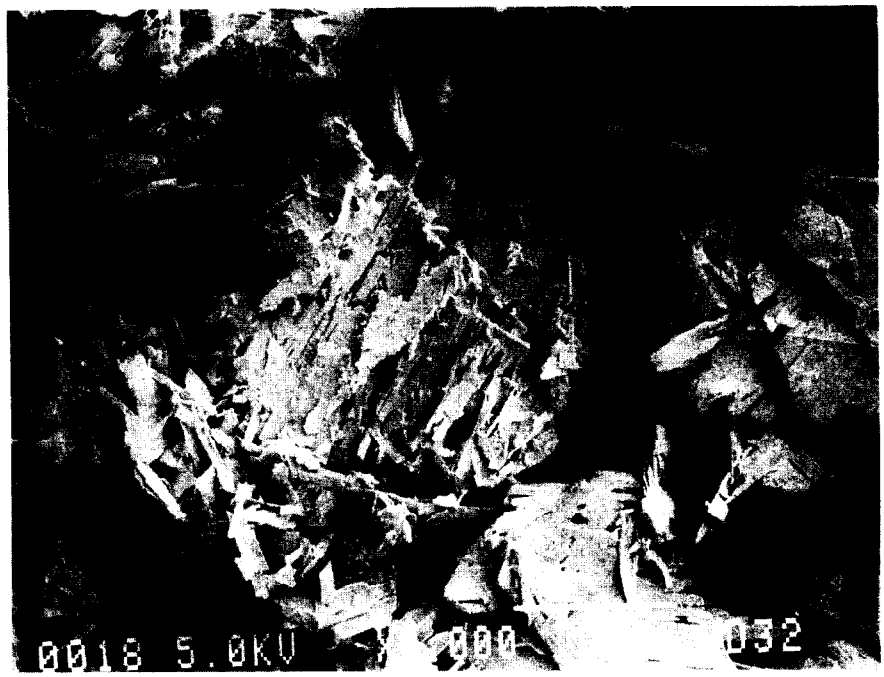

air

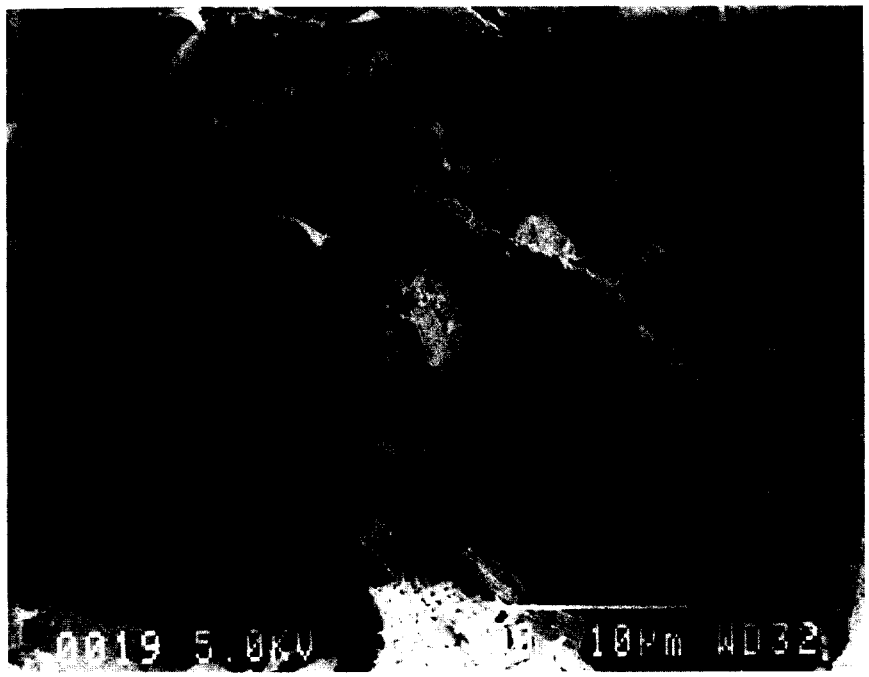

N_2

Fig. 5. (a) SEM of Ag_2NiO_2 obtained from the thermal decomposition of coprecipitate (2) in air and N_2 up to 500 C.

The oxides for example, obtained from the thermal decomposition of the solid solution of nickel $[Ag_2Ni(OX)_2 \cdot 2H_2O]$ in both air and N_2 were investigated by means of XRD and SEM. The patterns of the heated compound to 500°C in air and N_2 (Fig. 4) are mainly the same. Comparing the patterns with those of Ag_2O and NiO (ASTM cards no. 19-1155 and 22-1189) we can get the following results:

Fig. 5. (b) SEM of the heated mechanical mixture of silver oxalate and nickel oxalate (2a) up to 500°C.

(1) The pattern of the mixed oxide comprises of Ag_2O and NiO. The most intense line is that of Ag_2O (d = 2.35450°), whereas the lines of NiO (d = 2.40322, 2.08325 and 1.47303°) are weak. This indicates that the major phase is that of Ag_2O, which has been modified into a new phase due to the distribution of Ni^{2+} ions in the lattice. This is inferred from the appearance of two strong new lines at d = 2.03971 and 1.44303°.

(2) The most intense line of Ag_2O (d = 2.33000°) shifts to the higher side (d = 2.35450°) in the mixed oxide, whereas the lines of NiO (d = 2.41200, 2.08800 and 1.47700°) shift to the lower side. These shifts may be attributed to the formation of the mixed lattice.

The micrographs obtained from the SEM measurements of the mixed oxide obtained in air and N_2 are shown in Fig. 5(a). In the case of N_2, the micrograph consists of homogeneous thin sheet particles of varying particle size. In air, the micrograph displayed nearly the same type of particle morphology, along with smaller fragmented particles. The observed homogeneity of the particle morphology was lost in the micrograph of the mixed oxide obtained from the heated mechanical mixture of silver oxalate and nickel oxalate (2a) up to 500°C in N_2. As shown in Fig. 5(b), the micrograph consists of a mixture of two particle shapes and sizes. These results indicate that the mixed oxide (Ag_2NiO_2) obtained from the thermal decomposition of the compound (2) is a solid solution.

Acknowledgements—The author wishes to thank Professor Dollimore (Department of Chemistry, University of Toledo, U.S.A.) for the facilities provided in his laboratory to accomplish this work.

REFERENCES

1. Selvaray, U., Prosadarao, A. V., Komarneni, S., Brooks, K. and Kurtz, S., *J. Mater. Res.*, 1992, **7**, 992.
2. Bhattacharjee, S., Paria, M. K. and Maiti, H. S., *Mat. Lett.*, 1992, **13**, 130.
3. Gopalakrishna Murthy, H. S., Subba Rao, M. and Narayanan Kutty, T. R., *J. Inorg. Nucl. Chem.*, 1976, **38**, 417.
4. Vos, A., Mullens, J., Yperman, J., Franco, D. and Van Poucke, L. C., *Eur. J. Solid State Inorg. Chem.*, 1993, **30**, 929.
5. Macdonald, J. Y., *J. Chem. Soc.*, 1936, 832.
6. Griffith, R. L., *J. Chem. Phys.*, 1943, **11**, 499.
7. Dollimore, D. and Evans, T. A., *Thermochim. Acta*, 1991, **178**, 263.
8. Dollimore, D. and Evans, T. A., *Thermochim. Acta*, 1991, **179**, 49.
9. Gusev, E. A., Dalidovich, S. V., Shandakov, V. A. and Vecher, A. A., *Thermochim Acta*, 1985, **89**, 391.
10. Gao, X., Chen, D., Dollimore, D., Skrzypczak-Jankun, E. and Burckel, P., *Thermochim. Acta*, 1993, **220**, 75.
11. Figgis, B. N. and Martin, D. J., *J. Inorg. Chem.*, 1966, **5**, 100.
12. Gabelica, Z., Hubin, R. and Derouane, E. G., *Thermochim. Acta*, 1978, **24**, 315.
13. Wickham, D. G., *Inorg. Synth.*, 1967, **9**, 152.
14. Robin, J., *Bull. Soc. Chim. Fr.*, 1953, 1078.

15. Schuele, W. J., *J. Phys. Chem.*, 1959, **63,** 83.
16. Gallagher, P. K., *Thermochim. Acta*, 1993, **214,** 1.
17. Donia, A. M. and Dollimore, D., *Thermochim. Acta*, 1996, **290,** 139.
18. Goel, S. P. and Mehrotra, P. N., *J. Thermal Anal.*, 1985, **30,** 145.
19. Nakamoto, K., *Infrared Spectra of Inorganic and Coordination Compounds*. John Wiley, New York, 1970.
20. Gallagher, P. K. and Schrey, F., *J. Am. Ceram. Soc.*, 1964, **47,** 434.